Supporting Information

Svidritskiy et al. 10.1073/pnas.1304922110

SI Materials and Methods

Preparation of *Escherichia coli* Ribosomes and Ribosomal Ligands. Salt-washed 70S ribosomes were prepared from MRE600 *E. coli* as described (1). $tRNA^{Met}$ and $tRNA^{Phe}$ were purchased from MP Biomedicals and Chemical Block, respectively. *N*-Ac-Phe-$tRNA^{Phe}$ and elongation factor G (EF-G) with 6-hisitidine tag were prepared and purified as previously described (2-4). $tRNA^{fMet}$ (Chemical Block) was aminoacylated using [^{35}S]-labeled methionine (Perkin Elmer) and formylated as described (5). Cy5-labeled protein S6 and Cy3-labeled protein L9 were incorporated into 30S and 50S subunits by partial reconstitution from 30S and 50S subunits carrying S6 and L9 deletions, respectively, as previously described (6). The ΔS6 strain of *E. coli* from the Keio Collection was purchased from the Genetic Stock Center (Yale University). Doubly labeled 70S ribosomes were isolated using previously described procedures (6).

Filter-Binding Assay. Before filter-binding experiments, 70S ribosomes were incubated with excess M0-27 mRNA (GGC AAG GAG GUA AAA *AUG UAA* AAA AAA, IDT) in the presence or absence of blasticidin S (BlaS; Fischer Scientific) in Buffer A [20 mM Tris·HCl (pH 7.5), 100 mM NH_4Cl, 20 mM $MgCl_2$, 5 mM β-mercaptoethanol]. The 70S complex was prepared at 400 nM and incubated at 37 °C for 30 min with 600 nM [^{35}S]-N-formyl-methionyl-$tRNA^{fMet}$ (fMet-$tRNA^{fMet}$). The fraction of ribosome-bound [^{35}S]-fMet-$tRNA^{fMet}$ was assayed by nitrocellulose filter (Whatman 0.45 μM) binding as described (7) and quantified using a scintillation counter. The relative occupancy of the P site by [^{35}S]-fMet-$tRNA^{fMet}$ in the presence of blasticidin S (Fig. 1) is expressed as the ratio of cpm of the complex in the presence of the antibiotic to cpm obtained for [^{35}S]-fMet-$tRNA^{fMet}$-bound ribosomes not treated with the antibiotic. Filter-binding experiments at each concentration of BlaS were performed three times.

RF1-Mediated Release Assay and Puromycin Reaction. *E. coli* 70S ribosomes and [^{35}S]-fMet-$tRNA^{fMet}$ were prepared as described above. *E. coli* release factor 1 (RF1) incorporating a C-terminal hexahistidine tag was overexpressed and purified as described (8, 9). A 30 nM pretermination complex was formed by incubating [^{35}S]-fMet-$tRNA^{fMet}$ with an equimolar amount of 70S ribosomes and a 200-fold excess of M0-27 mRNA (IDT), resulting in positioning of the UAA termination codon in the ribosomal A site. To estimate BlaS inhibition constants for [^{35}S]-fMet release by RF1 and for the puromycin reaction, the assays were carried out at subsaturating concentrations of RF1 (80 nM) and puromycin (50 μM), at which the observed rate constants were at least twofold lower than at saturating concentrations. For the peptide release assay, the pretermination complex was added to RF1 and incubated at room temperature in 20 mM Tris·acetate (pH 6.5), 100 mM ammonium acetate, 20 mM magnesium acetate, and 5 mM β-mercaptoethanol. Aliquots were removed from the reaction at 10 time points and quenched in six volumes of 0.1 N HCl. Hydrolyzed [^{35}S]-fMet was extracted with 0.7 mL of ethyl acetate, 0.6 mL of which was added to scintillation mixture and counted using a scintillation counter. All reactions were performed at pH 6.5, at which the [^{35}S]-fMet background signal is lower than that at pH 7.5, whereas reaction rates are not substantially affected. Puromycin reactions were carried out using a similar approach except that aliquots were quenched in 1 M CH_3COONa (pH 5.5) saturated with $MgSO_4$. Time progress curves for RF1-mediated release and puromycin reactions were obtained in the presence of 0, 30, 60, 100, 150, 300, 800, and 2,000 nM blasticidin S and 10,000 nM blasticidin S for the puromycin reactions. Catalytic rates (k_{obs}) estimated by a single-exponential fit for each concentration of BlaS were then fit to a hyperbola, yielding the apparent inhibition constant K_i. It is noteworthy that the experimental setup limits the determination of apparent K_i to 30 nM (pretermination complex concentration) and thus may underestimate the inhibitory effect of BlaS on the termination reaction (apparent K_i = 32 ± 18 nM). All experimental data were obtained by repeating experiments at least two times. Curve fitting of experimental data were performed using GraphPad Prism (GraphPad Software).

FRET Measurements and Data Analysis. Ribosomal complexes were assembled as previously described (10) in polyamine buffer containing 30 mM Hepes (pH 7.5), 6 mM $MgCl_2$, 6 mM β-mercaptoethanol, 150 mM NH_4Cl, 0.1 mM spermine, and 2 mM spermidine. Ribosomal complexes with single tRNA bound in the P site were assembled by incubating 70S S6-Cy5/L9-Cy3 ribosomes (300 nM) with mRNA m291 (600 nM) annealed to a biotinylated primer (800 nM), and $tRNA^{Met}$, $tRNA^{Phe}$, or $tRNA^{fMet}$ (600 nM) at 37 °C for 20 min. Pretranslocation ribosomal complexes were assembled by incubating ribosomal complexes with a single $tRNA^{Met}$ bound in the P site with *N*-Ac-Phe-$tRNA^{Phe}$ (450 nM) at 37 °C for 30 min. Complexes were diluted in polyamine buffer to ∼1 nM and immobilized on quartz slides. The buffer was exchanged with polyamine buffer described previously with the addition of an oxygen-scavenging mixture consisting of 0.8 mg/mL glucose oxidase, 0.625% glucose, ∼1.5 mM 6-hydroxy-2,5,7,8-tetramethylchromane-2-carboxylic (Trolox, triplet-state quencher), and 0.03 mg/mL catalase to slow the occurrence of photobleaching.

Single-molecule FRET (smFRET) measurements were taken as previously described (10), using an Olympus IX71 microscope with a UPlanApo 60×/1.20W objective. Cy3 and Cy5 dyes were excited using 532 nm and 642 nm lasers, respectively (Spectra-Physics); total internal reflection was achieved using a quartz prism (ESKMA Optics). A DV2 (Photometrics) dual-view imaging system equipped with a 630 nm dichroic mirror was used to split the fluorescence into Cy3 and Cy5 channels, which was recorded using an Andor iXon+ EMCCD camera through the program Single (downloaded from Taekjip Ha's laboratory website at the University of Illinois at Urbana–Champaign, physics.illinois.edu/cplc/software) with exposure time set to 100 ms. Imaging was carried out at room temperature.

smFRET movies were processed using IDL and analyzed in MATLAB using scripts freely available online at physics.illinois.edu/cplc/software. Apparent FRET efficiencies (E_{app}) were calculated from the donor (I_{Cy3}) and acceptor (I_{Cy5}) fluorescence intensities by $E_{app} = I_{Cy5}/[I_{Cy5}+I_{Cy3}]$. FRET distribution histograms were constructed from traces that showed single-step photobleaching events for both Cy5 and Cy3 using a Matlab script generously provided by Peter Cornish (University of Missouri, Columbia). Traces were normalized by length so that each trace contributes to a frequency count of 1. All histograms were smoothed with a five-point window and fit to the sum of two Gaussians. The peak positions were left unrestrained. The widths of the Gaussians were self-consistent and the residuals were random. Because less than 50% of the data for each set contained at least five transitions, data were not suitable for Hidden Markov modeling analysis (11, 12). The kinetic rates of transitions were determined by dividing the total number of transitions from one state to another by the total amount of time spent in the initial state.

Stopped-Flow Measurements of Presteady-State Translocation Kinetics. Kinetics of mRNA translocation was measured as previously described (12-15) with minor modifications. Pretranslocation complexes were constructed by incubation of 70S ribosomes (1 μM) with fluorescein-labeled mRNA (5′-GGC AAG GAG GUA AAA AUG UUU AAA-3′-fluorescein, synthesized by Dharmacon RNAi Technologies, 0.85 μM) and deacylated $tRNA^{Met}$ (2 μM) in polyamine buffer (20 mM Hepes·KOH, pH 7.5, 6 mM $MgCl_2$, 150 mM NH_4Cl, 6 mM β-mercaptoethanol, 2 mM spermidine, 0.1 mM spermine) for 20 min at 37 °C followed by incubation with *N*-acetyl-Phe-$tRNA^{Phe}$ (1.5 μM) for 30 min at 37 °C. Pretranslocation ribosomes were mixed with WT EF-G and GTP using an Applied Photophysics stopped-flow fluorometer. Final concentrations after mixing were: 35 nM ribosomes, 1.4 μM EF-G, and 0.5 mM GTP. Fluorescein was excited at 490 nm and fluorescence emission was detected using a 515 nm long-pass filter. Monochromator slits were adjusted to 9.3 nm. All stopped-flow experiments were done at 23 °C. Translocation of mRNA resulted in partial quenching of fluorescein coupled to the 3′ end of mRNA. Approximately 10 time traces were accumulated for each experiment. Time traces were analyzed using Pro-Data-Viewer software (Applied Photophysics). As has been reported previously (13–15), the kinetics of mRNA translocation are clearly biphasic and are best fitted by the sum of two exponentials, corresponding to apparent rate constants k_1 and k_2 (Table S2). Although the biphasic character of fluorescence changes associated with mRNA translocation is well documented (12), the physical basis of this phenomenon remains unclear. The rate of translocation was defined as the weighted average rate constant k_{av}, calculated as the sum of k_1 and k_2 normalized to their respective contributions to the total amplitude of fluorescence change [$k_{av} = (k_1{*}A_1 + k_2{*}A_2)/(A_1 + A_2)$] (12).

Crystal Structure Determination. 70S ribosomes were purified from wt *Thermus thermophilus* HB27 as described (8). A total of 4 μM ribosomes (final concentration) was incubated with twofold molar excess of $tRNA^{fMet}$ (Chemical Block), fivefold excess M0-27 mRNA (IDT), and 1 mM BlaS in buffer containing 25 mM Tris·acetate (pH 7.0), 50 mM potassium acetate, 10 mM ammonium acetate, and 10 mM magnesium acetate. Crystallization drops were formed by mixing 1.2 μL of the 70S·M027·$tRNA^{fMet}$·BlaS complex with 1.2 μL crystallization buffer [0.1 M Tris·HCl (pH 7.5), 4% (vol/vol) PEG 20000, 8% (vol/vol) 2-Methyl-2,4-pentanediol, and 0.2 M KSCN]. Crystallization was carried out by hanging-drop vapor diffusion using 0.5–0.8 M NaCl as reservoir solution. Cryoprotection was performed as described (9). Crystals were flash frozen by plunging into liquid nitrogen.

Crystals were screened at beam lines 23ID-B and 23ID-D at the Advanced Photon Source at Argonne National Laboratory and beam line X25 at the National Synchrotron Light Source at Brookhaven National Laboratory. Diffraction data were collected at beam line X25 at the NSLS using the PILATUS 6M PAD detector at an X-ray wavelength of 1.1 Å and an oscillation angle of 0.2°. For determining the structure of the 70S·M027·$tRNA^{fMet}$·BlaS complex, one dataset obtained from a single crystal was integrated and scaled using XDS. Two percent of the unique reflections were marked as test-set (R^{free} set) reflections and used for cross-validation throughout refinement. A previously determined X-ray structure of the 70S·RF2 termination complex obtained from the same crystal form (9) was used as a starting model for molecular replacement with tRNA, mRNA, and RF2 molecules removed. Density for tRNA, mRNA, and BlaS was clearly visible in initial F_{obs}-F_{calc} and $3F_{obs}$-$2F_{calc}$ difference maps. The BlaS molecule was built into difference density using the structural model from Protein Data Bank 1KC8 (16). Structure refinement was carried out using PHENIX (17) and CNS (18, 19) as described (9) and yielded a structure with R/R^{free} of 0.232/0.268 (Table S3). Superposition of 70S structures was performed by aligning 23S ribosomal RNA in PyMOL (20). Figures were rendered using PyMOL. The atomic coordinates and structure factors have been deposited in the Protein Data Bank (PDB ID codes 4L6J, 4L6K, 4L6L, and 4L6M).

1. Moazed D, Noller HF (1986) Transfer RNA shields specific nucleotides in 16S ribosomal RNA from attack by chemical probes. *Cell* 47(6):985–994.
2. Moazed D, Noller HF (1989) Intermediate states in the movement of transfer RNA in the ribosome. *Nature* 342(6246):142–148.
3. Wilson KS, Noller HF (1998) Mapping the position of translational elongation factor EF-G in the ribosome by directed hydroxyl radical probing. *Cell* 92(1):131–139.
4. Walker SE, Fredrick K (2008) Preparation and evaluation of acylated tRNAs. *Methods* 44(2):81–86.
5. Lancaster L, Noller HF (2005) Involvement of 16S rRNA nucleotides G1338 and A1339 in discrimination of initiator tRNA. *Mol Cell* 20(4):623–632.
6. Ermolenko DN, et al. (2007) Observation of intersubunit movement of the ribosome in solution using FRET. *J Mol Biol* 370(3):530–540.
7. Spiegel PC, Ermolenko DN, Noller HF (2007) Elongation factor G stabilizes the hybrid-state conformation of the 70S ribosome. *RNA* 13(9):1473–1482.
8. Laurberg M, et al. (2008) Structural basis for translation termination on the 70S ribosome. *Nature* 454(7206):852–857.
9. Korostelev A, et al. (2008) Crystal structure of a translation termination complex formed with release factor RF2. *Proc Natl Acad Sci USA* 105(50):19684–19689.
10. Cornish PV, Ermolenko DN, Noller HF, Ha T (2008) Spontaneous intersubunit rotation in single ribosomes. *Mol Cell* 30(5):578–588.
11. Studer SM, Feinberg JS, Joseph S (2003) Rapid kinetic analysis of EF-G-dependent mRNA translocation in the ribosome. *J Mol Biol* 327(2):369–381.
12. Ermolenko DN, Noller HF (2011) mRNA translocation occurs during the second step of ribosomal intersubunit rotation. *Nat Struct Mol Biol* 18(4):457–462.
13. Munro JB, et al. (2010) Spontaneous formation of the unlocked state of the ribosome is a multistep process. *Proc Natl Acad Sci USA* 107(2):709–714.
14. Peske F, Savelsbergh A, Katunin VI, Rodnina MV, Wintermeyer W (2004) Conformational changes of the small ribosomal subunit during elongation factor G-dependent tRNA-mRNA translocation. *J Mol Biol* 343(5):1183–1194.
15. Shi X, Chiu K, Ghosh S, Joseph S (2009) Bases in 16S rRNA important for subunit association, tRNA binding, and translocation. *Biochemistry* 48(29):6772–6782.
16. Hansen JL, Moore PB, Steitz TA (2003) Structures of five antibiotics bound at the peptidyl transferase center of the large ribosomal subunit. *J Mol Biol* 330(5):1061–1075.
17. Adams PD, et al. (2002) PHENIX: Building new software for automated crystallographic structure determination. *Acta Crystallogr D Biol Crystallogr* 58(Pt 11):1948–1954.
18. Brünger AT, et al. (1998) Crystallography & NMR system: A new software suite for macromolecular structure determination. *Acta Crystallogr D Biol Crystallogr* 54(Pt 5):905–921.
19. Brünger AT, Adams PD, Rice LM (1997) New applications of simulated annealing in X-ray crystallography and solution NMR. *Structure* 5(3):325–336.
20. DeLano, WL (2002) The PyMOL Molecular Graphics System (DeLano Scientific, Palo Alto, CA).

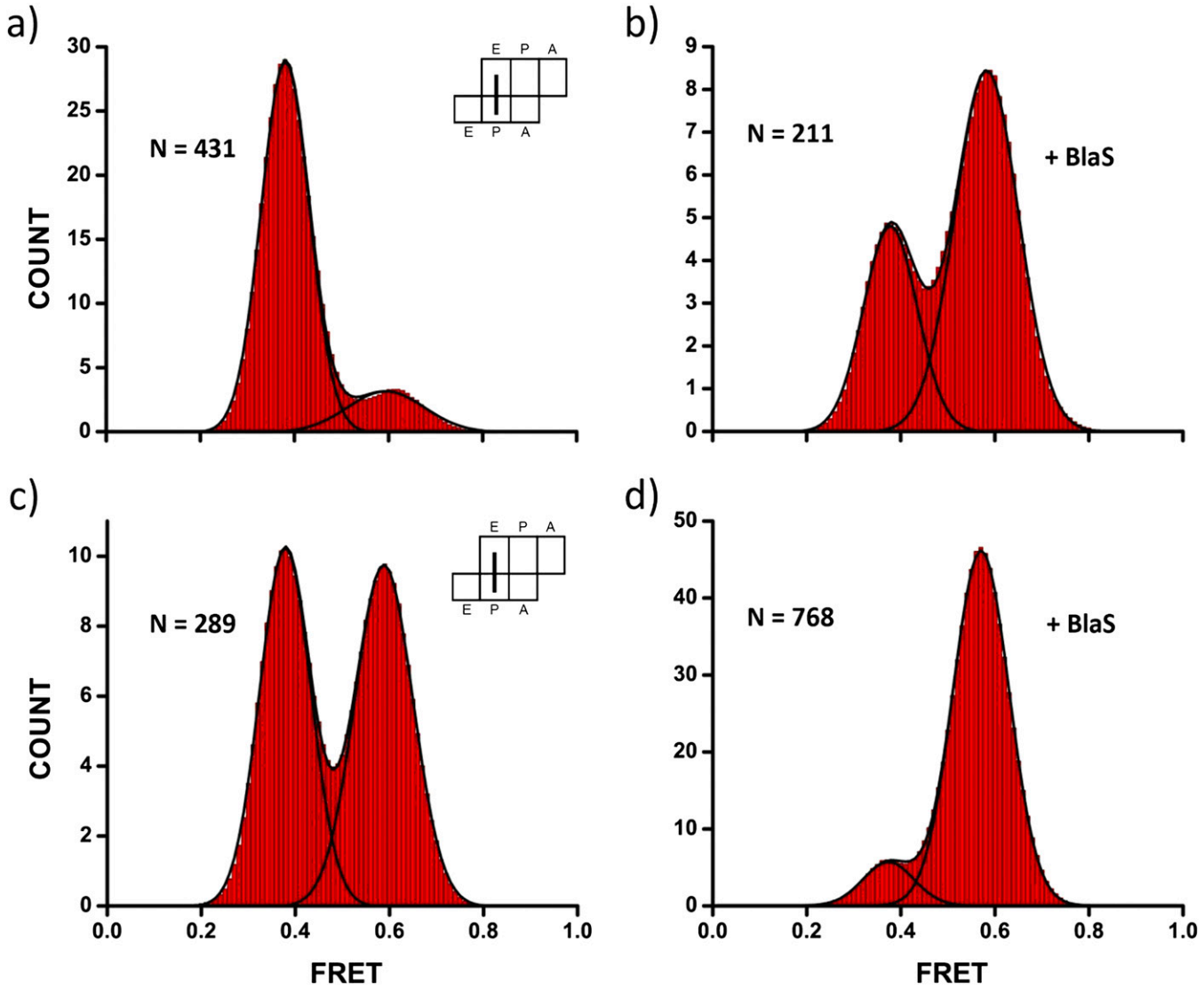

Fig. S1. BlaS inhibits counterclockwise rotation of the 30S subunit coupled to the movement of deacylated $tRNA^{Met}$ or $tRNA^{fMet}$ into the hybrid P/E state. Histograms showing distributions of FRET values in ribosomes containing deacylated $tRNA^{Met}$ (*A* and *B*) or deacylated $tRNA^{fMet}$ (*C* and *D*) in the P site in the absence (*A* and *C*) or presence of BlaS (*B* and *D*). N, number of single-molecule FRET traces compiled.

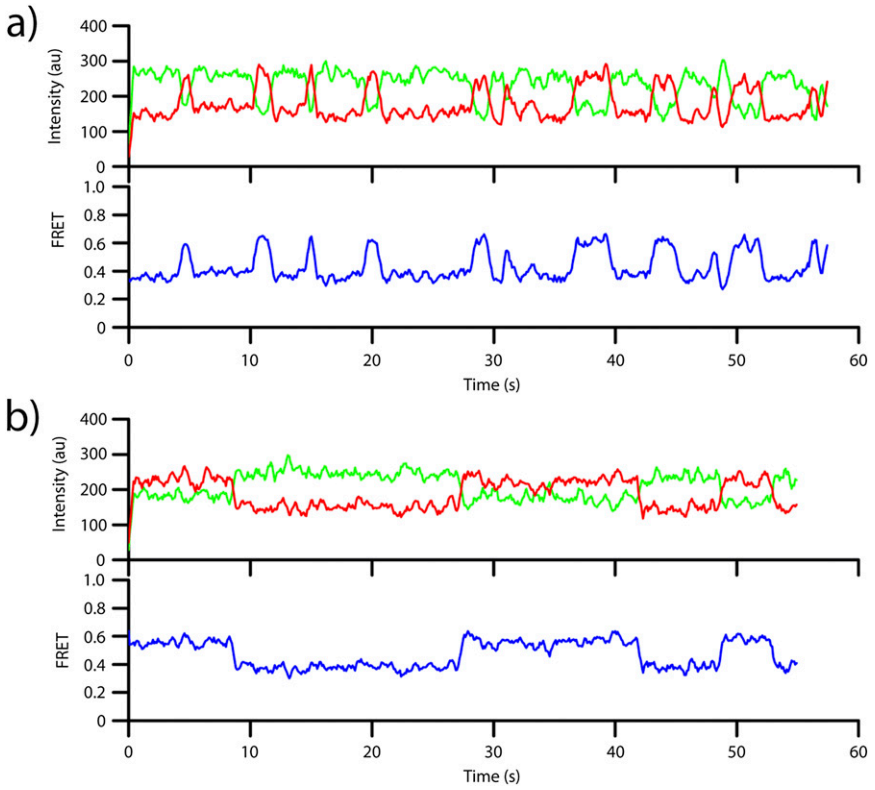

Fig. S2. Representative time traces of 70S ribosomes containing S6-Cy5 and L9-Cy3 with $tRNA^{Met}$ in the P site and *N*-Ac-Phe-$tRNA^{Phe}$ in the A site imaged in the absence (*A*) or presence (*B*) of BlaS. Cy3 and Cy5 fluorescence intensities are represented by green and red traces, respectively. Calculated FRET is shown as the blue trace.

Table S1. Proportions of rotated and nonrotated ribosomes and rates of spontaneous rotation in the presence and absence of BlaS derived from smFRET

70S complex	Percent NR	Percent R	$k_{0.6\rightarrow0.4}$, s^{-1}	$k_{0.4\rightarrow0.6}$, s^{-1}	K_{eq} (rates)	K_{eq}, %R/%NR	Percent trans
Deacylated tRNA in P site							
$tRNA^{Phe}$	32	68	0.87	0.23	3.8	2.1	51
$tRNA^{Phe}$ with BlaS	78	22	0.19	0.28	0.7	0.3	24
$tRNA^{Met}$	15	85	0.62	0.17	3.7	5.7	34
$tRNA^{Met}$ with BlaS	67	33	0.14	0.14	1.0	0.5	43
Pretranslocation complexes							
$tRNA^{Met}$/*N*-Ac-Phe-$tRNA^{Phe}$	28	72	0.90	0.29	3.1	2.6	33
$tRNA^{Met}$/*N*-Ac-Phe-$tRNA^{Phe}$ with BlaS	41	59	0.14	0.07	2.0	1.4	37

Percent of pretranslocation ribosomes in nonrotated (NR), 0.6 FRET state or rotated (R), 0.4 FRET state derived from FRET distribution histograms (Figs. 2 and 3). SD was 5%. Rates of counterclockwise ($k_{0.6\rightarrow0.4}$) and clockwise ($k_{0.4\rightarrow0.6}$) intersubunit rotation are calculated as number of transitions/dwell time. Equilibrium constants (K_{eq}) were calculated from the ratio of rates for forward and reverse rotation. These values deviate somewhat from equilibrium constants calculated from the relative populations of rotated and nonrotated ribosomes (K_{eq}, %R/%NR) because of the presence of a fraction of ribosomes that do not display fluctuations in smFRET time traces and thus skew equilibrium constant values derived from the distribution histogram. The percentage of traces with fluctuations (percent trans) is defined as the total number of traces that contain at least one FRET transition between 0.6 and 0.4 FRET states divided by the total number of traces.

Table S2. Rates of EF-G-mediated mRNA translocation in the absence and presence of BlaS

	k_1, s^{-1}	k_2, s^{-1}	$A_1/(A_1+A_2)$	k_{av}, s^{-1}
EF-G-GTP	6.0 ± 0.9	0.5 ± 0.1	0.56 ± 0.05	3.7 ± 0.6
EF-G-GTP + 1 mM BlaS	5.2 ± 0.7	0.4 ± 0.1	0.46 ± 0.01	2.6 ± 0.4

Kinetics of mRNA translocation was measured in presteady-state stopped-flow kinetic experiments by quenching of fluorescein attached to the mRNA (Fig. 3C). k_1 and k_2 are the rate constants of double-exponential fits of the mRNA translocation data; $A_1/(A_1+A_2)$ is the relative contribution of the faster phase to the total amplitude of fluorescein quenching. Weighted average values (k_{av}) for mRNA translocation rates were calculated by combining the rate constants derived from the double-exponential fits: $k_{av} = (k_1A_1 + k_2A_2)/(A_1 + A_2)$. The rates of both the fast (k_1) and slow (k_2) phases of translocation were not significantly affected by BlaS. However, in the presence of BlaS, the amplitude of the slow phase increased at the expense of the fast phase, resulting in a small decrease in k_{av}.

Table S3. Data collection and refinement statistics

	Statistics
Data collection	
Space group	$P2_12_12_1$
Cell dimensions	
a, *b*, *c*; Å	211.53, 454.44, 620.87
α, β, γ; °	90, 90, 90
Resolution, Å	70-3.4 (3.4–3.53)*
$R_{p.i.m.}$[†]	0.158 (0.88)
CC(1/2)[‡]	99.3 (37)
I/σ*I*	7.44 (1.01)[§]
Completeness, %	100 (100)
Redundancy	9.9 (10)
Refinement	
Resolution, Å	50–3.4
No. reflections	810,608
R^{work}/R^{free}	0.232/0.268
No. atoms	293,128
Ions modeled as Mg^{2+}	4,363
rmsd	
Bond lengths, Å	0.003
Bond angles, °	0.618

*Values in parentheses are for the high-resolution shell.
[†]$R_{p.i.m.}$, precision-indicating merging R factor (1) was calculated using SCALA (2).
[‡]CC(1/2) is the percentage of correlation between intensities from random half-datasets as defined by Karplus and Diederichs (3).
[§]I/σI = 2.0 at 3.65 Å.

1. Weiss MS (2001) Global indicators of X-ray data quality. *J Appl Cryst* 34(2):130–135.
2. Collaborative Computational Project, Number 4 (1994) The CCP4 suite: programs Programs for protein crystallography. *Acta Crystallogr D Biol Crystallogr* 50(Pt 5):760–763.
3. Karplus PA, Diederichs K (2012) Linking crystallographic model and data quality. *Science* 336(6084):1030–1033.